Markov Model-Based Energy Storage System Planning in Power Systems

Ying-Yi Hong, *Senior Member, IEEE*, and Man-Yin Wu

***Abstract*—Battery energy storage systems (BESSs) can regulate the supply of energy from an electric utility, and improve the reliability and stability of the power system, which has high penetration of renewable power generation. This paper determines the optimal sizes (MWh) and capacities (MW) of BESSs in a distribution system that is composed of photovoltaic (PV) arrays. The objective is to minimize the investment cost, replacement cost, operation/maintenance cost, and the net present values of both the energy loss cost and to maximize the annual arbitrage benefit (AAB). The energy loss cost and AAB incorporate time-of-use (TOU) tariffs. The objective is subject to equality constraints (power flow equations and chronological ESS balance constraints) and inequality constraints (voltage, line flow, and BESS operational limits). Because the studied problem involves many constraints and variables in the chronological domain, traditional optimization methods cannot be applied directly to this large-scale problem. Assume that the chronological PV powers and loads are stochastic process, where the description of present state fully contains the information for the future evolution. Thus, Markov models are implemented by considering probability/duration/frequency of PV powers and loads to reduce the numbers of constraints and variables. The Markov states are attained using a clustering algorithm that is based on fuzzy-c-means. Simulation results obtained from a 33-bus system consisting of a 1 MW PV farm and six BESSs reveal the applicability of the proposed method. Simulation results indicate that the TOU tariff markedly affects the allocation of BESSs and the AAB benefit is generally smaller than the costs of the BESSs and energy losses.**

***Index Terms*—Clustering, energy storage system, markov model, optimization.**

NOMENCLATURE

Indices:

h	Hour index; $h = 1, 2, \ldots, 8760$.
i, j	Bus index; $i, j = 1, 2, \ldots, Nbus$.
m	State index; $m = 1, 2, \ldots, M$.
n	BESS index; n $= 1, 2, \ldots, NB$.
s_1 and s_2	State indices for PV and demand. $s_1 = 1, 2, \ldots, C1$; $s_2 = 1, 2, \ldots, C2$.
y	Year index.

Parameters:

α	A fuzzifier determining the level of cluster fuzziness.
C	A given number of clusters.
C_E	Energy unit cost for BESS (305 \$/kWh).
C_M	Annual maintenance and operation cost (15 \$/kW).
C_P	Capacity unit cost (175 \$/kW).
C_{pk} and C_{ofk}	Electricity tariffs for the peak (27 \$/MWh) and off-peak (18\$/MWh) loads.
C_R	NPV of replacement cost (\$/kWh) in (4).
$d(s)$	Duration of scenario s.
F	Inflation rate (5%).
FR	Future value of the replacement price (30 \$/kW).
$f(s)$	Frequency of scenario s.
Hdis and Hch	Known sets of hours for discharging and charging.
IR	Interest rate (10%).
LIR	Rate of increase of the annual loss (1.05).
N	Known number of datasets for clustering.
NB	Total number of BESSs ($NB = 6$).
$Nbus$	Number of system buses.
Ny	Number of years in the planning period (20).
η	Charging efficiency (85%) of the BESS.
r	Replacement period (5 years).
Sdis and Sch	Sets of discharging and charging scenarios.
Tdis and Tch	Known total discharging and charging periods (in hours).
Y_{ij} and θ_{ij}	Magnitude and phase angle of element between buses i and j in the system admittance matrix.

Variables:

CEloss	Cost of the energy losses.
$E_B^r(n)$	Rated energy (kWh) of the nth BESS.
$E_B(n,h)$	Energy (MWh) stored in the nth BESS at hour h.
lf_{ij}	Line flow between buses i and j.
$p(s)$	Probability of scenario s.
$P_B^{dis}(n,h)$; $P_B^{ch}(n,h)$	Discharging and charging powers in the nth BESS in hour h.
$P_B^{dis}(n,s)$; $P_B^{ch}(n,s)$	Discharging and charging powers in the nth BESS for scenario s.
$P_B^r(n)$	Rated capacity (kW) of the nth BESS.
P_{D_i}	Demand at bus i.

Manuscript received July 16, 2018; revised December 6, 2018; accepted February 12, 2019. Date of publication March 11, 2019; date of current version November 22, 2019. This work was supported by the Ministry of Science and Technology (Taiwan) under Grant MOST 107-2221-E-033-056. *(Corresponding author: Ying-Yi Hong.)*

The authors are with the Department of Electrical Engineering, Chung Yuan Christian University, Taoyuan 32023, Taiwan (e-mail: mm1223s@yahoo.com.tw; yyhong@ee.cycu.edu.tw).

Digital Object Identifier 10.1109/JSYST.2019.2900081

P_{G_i}	Injected real power, including photovoltaic power, at bus *i*.
$P_{PV}(s_1)$	PV power generation at state s_1.
$P_D(s_2)$	Power demand at state s_2.
Ploss(*h*)	Power loss at a specific hour *h*.
Pb_m	Probability for a state *m*.
$\mu_c(\zeta)$	Value of the membership function that relates V_c to X_ζ.
V and δ	Magnitude and phase angle of bus voltage.
V_c	Unknown central vector of the cth cluster
X_ζ	ζth known dataset for clustering.

I. Introduction

SMART power grids need many new technologies to change the traditional power grid into a more distributed customer-driven grid [1]. On this way, electric vehicles, distributed photovoltaic (PV) arrays and wind-turbine-generators (WTGs), battery energy storage systems (BESSs) and many other technologies have emerged. Balancing the uncertain demand side and fluctuating generation of renewables becomes an essential issue in a smart grid [2], [3]. A review of resource management schemes in a smart grid with non-deterministic load and generation was given in [4]. Renewable power generation from PV arrays and WTGs are attracting much attention because of their usefulness in satisfying the increasing demand for electricity while mitigating greenhouse gas emissions [5], [6]. However, power generation from the PV arrays and WTGs is uncertain and intermittent. To solve this problem, BESSs are used to mitigate the impact of sudden variations of PV power and the intermittent fluctuations of WTG power on the power system operation [7]–[9]. BESSs can also provide voltage support [10], regulate system frequency [11], improve reliability [12], and reduce load shedding [13].

The size (MWh) and capacity (MW) of a BESS are determined in the planning stage by considering different factors. The power systems for sizing the BESS may be grid-tied and stand-alone. Daghi *et al*. presented a four-layer procedure that considered the uncertainty of battery characteristics, load and wind power in an active distribution network [14]. They used a genetic algorithm to determine the locations, capacities, and power ratings of batteries and simulated annealing to determine the charge/discharge power of the batteries in each hour [14]. Mahani *et al*. proposed a network-aware approach to BESS planning and control in a network with a high penetration of renewables; they utilized the high-dimensional data clustering method to reduce the size of the studied dataset [15]. Li *et al*. determined the installation locations and the initial capacities of BESSs using the loss sensitivity factor approach, and then identified the optimal installation capacities of BESSs to maximize the investment benefits and to minimize line losses [16]. Gitizadeh and Fakharzadegan considered the adoption of time-of-use (TOU) pricing using mixed integer programming to implement load shifting and peak shaving [17]. Hemmati *et al*. determined the capacities and charging/discharging regimes of BESSs to tackle uncertainty associated with wind-solar units as well as to relieve congestion in the lines [18]. Kim proposed a power-flow algorithm to optimize the reactive power to be either consumed or injected by PV systems and a hybrid multi-objective sensitivity algorithm that optimized the capacity of PV and storage systems [19]. Awad *et al*. proposed a methodology for allocating BESSs in distribution systems to defer system upgrades, minimize system losses, and exploit the arbitrage benefit [20]. Tang proved that BESSs are optimally placed near the leaves of the network and away from substations in order to minimize losses [21]. Giannitrapani *et al*. presented a clustering and sensitivity algorithm to allocate the BESSs for voltage control in distribution systems [22].

According to the above descriptions, existing methods for sizing the BESSs in a distribution system at least have one of the following limitations.

1) The electricity tariffs or TOU price were neglected [15], [16], [18], [19], [21], [22]. When a BESS is operated in a distribution system, all energies from the utility grid, renewables, and BESS must be coordinated. This tariff or price becomes a crucial factor that affects the sizes and capacities of the BESSs.
2) The power network was not considered [14], [15]. The reverse power flow and voltage profile, which are regulated by the BESSs, have to be addressed in the distribution system; otherwise, the studied problem is the same as the one in a standalone microgrid.
3) The number of studied scenarios was limited [14], [16], [18], [19], [21], [22]. The sizing problem is associated with a planning study, and differs from an operation problem. Sufficient representative scenarios must be taken into account.
4) The control scheme of the BESS was not investigated [15], [16], [18], [19]. Specifically, the charging/discharging of a BESS depends on not only electricity tariffs but also its state-of-charge (SOC).
5) The net present value (NPV) or capital recovery factor was not considered [19], [21], [22]. Different energy resources (renewables, BESSs, and the utility grid) have different lifetimes, which need to be considered.

Based on the above discussion, this paper presents a novel method to determine the MWh and MW of the BESSs in a distribution system. The charging/discharging scheme of a BESS follows the TOU tariffs of the utility. The problem is solved by an optimization that involves power flow equations (equality constraints) and voltage/line flow limits and SOC limit (inequality constraints). The studied scenarios are acquired using Markov models of PV powers and loads.

The contributions of this paper are summarized as follows.

1) The historical chronological hourly PV powers and loads are converted to Markov states. The studied scenarios are generated by integrating these different Markov states.
2) The many chronological constraints/variables are transformed into a small number of scenario-based constraints/variables. Accordingly, the optimal sizes (MWh) and capacities (MW) of BESSs in a distribution system can be obtained using optimization method in a fairly time.

3) Only a single optimization run is conducted to study multiple scenarios. Individual optimizations for all scenarios can be avoided on account of Markov chain for both PV powers and loads.

The rest of the paper is organized as follows. Section II presents a detailed description and formulation of the problem. Section III presents the proposed method for solving the problem. Section IV presents the results of simulations. Section V draws conclusions

II. Problem Description and Formulation

A. Problem Description

The studied problem involves some essential considerations.

1) A BESS requires much more space than shunt capacitors in the substations (buses) owing to their indoor cooling and control. Accordingly, the candidate buses for BESS allocation are specified herein.
2) The utility or distribution company, rather than the procumers (end-users), owns the BESSs. Thus, the utility or distribution company can consider all BESSs at the same time.
3) Energy is preferably stored when the electricity tariff is low in off-peak periods, and produced when the electricity tariff is high in peak periods. Thus, BESS can be used to increase the annual arbitrage benefit.
4) The states (charging and discharging) of a BESS depend on the system load; advanced forecasting techniques and controllers are not required. Specifically, if the system load exceeds a certain level (threshold), then the BESS discharges; otherwise, it charges. Thus, the BESS can shave the peak load and fill the off-peak load.
5) The bus voltages, line flows and losses must be evaluated by performing power flow studies. The distribution system loss can be reduced by the provision of energy from the local BESS to the local bus load.
6) The BESS is priced in \$/MWh and \$/MW. The "\$/MWh" price is related to the size of the BESS while the "\$/MW" price is affected by the ancillary facilities for the BESS, such as power electronics.
7) Different energy resources (renewable and BESS) have different lifetimes. Renewables and BESSs require initial investments and no fuel, but a utility has fuel costs, which must be considered in the studied period. NPV, which is a measurement of profit that is calculated by subtracting the present values of cash outflows (including initial cost) from the present values of cash inflows over a period, must be taken into account.

B. Problem Formulation

According to the above description, the problem of interest can be solved by minimizing an objective as follows:

$$\text{Min} \sum_{n=1}^{NB} \{(C_P + C_M \times \text{PVF}) \times P_B^r(n) + (C_E + C_R) \times E_B^r(n)\} + \text{NPV}_{\text{LO}} - \text{NPV}_{\text{AR}} \quad (1)$$

where NPV_{LO} and NPV_{AR} are the net present values of the loss and annual arbitrage benefit, respectively.

Specifically, the present value function can be expressed as follows [23], [24]:

$$\text{PVF} = \frac{(1+\text{EIR})^{Ny} - 1}{\text{EIR}(1+\text{EIR})^{Ny}} \quad (2)$$

where EIR is the effective interest rate as follows:

$$\text{EIR} = \frac{IR - F}{1+F}. \quad (3)$$

The NPV of the replacement cost of a BESS is

$$C_R = \frac{FR}{(1+\text{EIR})^r}. \quad (4)$$

The NPV of the energy loss cost can be estimated as follows:

$$\text{NPV}_{\text{LO}} = \sum_{y=1}^{Ny} \frac{(\text{LIR})^{y-1} \times \text{CEloss}}{(1+\text{EIR})^y}. \quad (5)$$

CEloss can be evaluated further from the loss (Ploss(*h*)) at a specific hour (*h*) as follows:

$$\text{CEloss} = \sum_{h \in \text{Hdis}} \text{Tdis} \cdot \text{Ploss}(h) \cdot C_{pk} + \sum_{h \in \text{Hch}} \text{Tch} \cdot \text{Ploss}(h) \cdot C_{opk}. \quad (6)$$

Then, the NPV of the arbitrage benefit (NPV_{AR}) can be evaluated as follows:

$$\left[\sum_{n=1}^{NB}\left(\sum_{h \in \text{Hdis}} P_B^{\text{dis}}(n,h)\, C_{pk} - \sum_{h \in \text{Hch}} \frac{P_B^{\text{ch}}(n,h)}{\eta} C_{opk}\right)\right] \cdot \text{PVF}. \quad (7)$$

The above objective is subject to two classes of equality constraints, which are hourly power flow equations and energy balance constraints. For bus *i* (with a BESS), the real power flow equation is (8) or (9), depending on its status (charging or discharging)

$$P_{G_i} - P_{D_i} - P_{B_i}^{\text{ch}} = \sum_{j=1}^{N\text{bus}} V_i \cdot V_j \cdot Y_{ij} \cdot \cos(\theta_{ij} + \delta_i - \delta_j) \quad (8)$$

$$P_{G_i} - P_{D_i} + P_{B_i}^{\text{dis}} = \sum_{j=1}^{N\text{bus}} V_i \cdot V_j \cdot Y_{ij} \cdot \cos(\theta_{ij} + \delta_i - \delta_j). \quad (9)$$

For the *n*th BESS, the energy balance constraint between hours *h* and $h+1$ is

$$E_B(n, h+1) = E_B(n,h) + \eta \cdot P_B^{\text{ch}}(n,h) - P_B^{\text{dis}}(n,h). \quad (10)$$

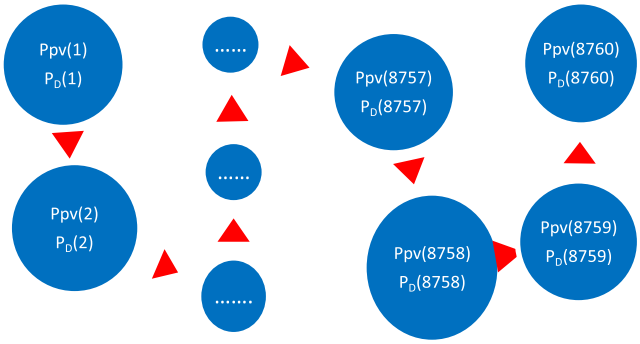

Fig. 1. Chronological time series from $h = 1$ to $h = 8760$.

The objective in (1) is also subject to the following inequality constraints:

$$0 \le E_B^r(n) \le E_B^{\max}(n) \tag{11}$$

$$E_B^{\min}(i) \le E_B(n,h) \le E_B^r(n) \tag{12}$$

$$0 \le P_B^r(n) \le P_B^{\max}(n) \tag{13}$$

$$0 \le P_B^{dis}(n,h) \le P_B^r(n) \tag{14}$$

$$0 \le P_B^{ch}(n,h) \le P_B^r(n) \tag{15}$$

$$V_i^{\min} \le V_i(h) \le V_i^{\max} \tag{16}$$

$$lf_{ij}^{\min} \le lf_{ij}(h) \le lf_{ij}^{\max}. \tag{17}$$

The superscripts "max" and "min" signify the maximum and minimum, respectively. The maximums of the capacity and energy for a single BESS are 1 MW and 1 MWh herein, respectively. The superscript "*r*" indicates the rated P_B or E_B.

The unknowns in (1)–(17) include hourly voltages and phase angles in the power flow equations, $E_B^r(n)$, $P_B^{\text{dis}}(n,h)$, $P_B^{\text{ch}}(n,h)$, and $P_B^r(n)$. The hourly power flow equations concerning hourly loads and power generation from photovoltaic arrays (8760 h in one year) are considered to cover different daily load and PV power profiles. The dependent variables consist of $E_B(n,h)$, Ploss(*h*), and $lf_{ij}(h)$, $h = 1, 2, \ldots, 8760$ and $n = 1, 2, \ldots, 6$ herein. The computational resources that are required to solve the above problem are prohibitive because the above formulation involves an extreme number of constraints and unknowns.

III. Proposed Method

The problem that is expressed in Section II is a large-scale nonlinear optimization problem. Solving this problem is computationally prohibitive on account of the extremely large number of chronological variables and constraints. In this paper, this chronological problem is converted into a Markov-based problem, in which the probability, duration, and frequency of PV power and load are considered. Specifically, as shown in Fig. 1, a traditional chronological time series is used, with increasing hours from $h = 1$ to $h = 8760$ in order. When the Markov model is used, the conditions of the power system vary among scenarios that are specified by various datasets (photovoltaic power P_{PV} and load demand P_D), according to two transition rates,

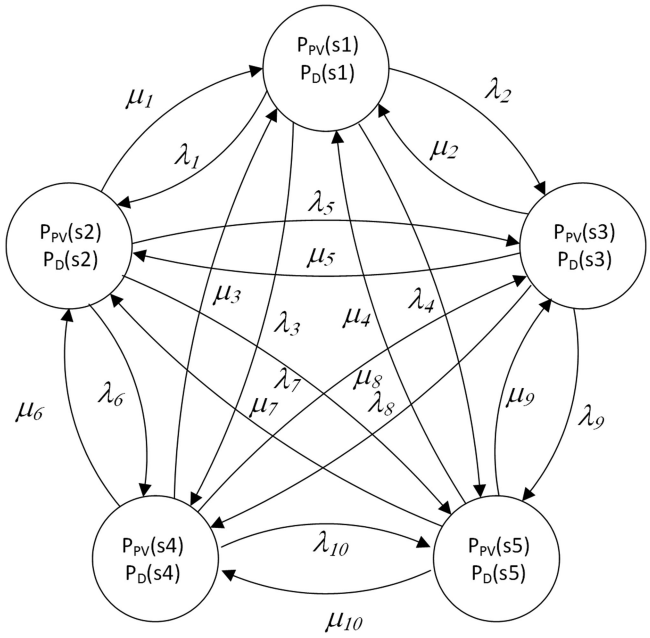

Fig. 2. Five-scenario power system.

the failure rate (λ), and the repair rate (μ). Fig. 2 illustrates a five-scenario power system. Each chronological parameter is converted to its corresponding state with its own probability, duration, and frequency. The integration of all states yields scenarios. The Markov models substantially reduce the numbers of variables and constraints.

A. Fuzzy-c-Means (FCM)

The Markov states can be obtained using a fuzzy-c-means (FCM) algorithm. The operational states in terms of the PV power generation and load have to be discretized to $P_{PV}(s_1)$ and $P_D(s_2)$.

Each dataset (vector) of PV powers or loads has a degree (membership function) that is correlated with a cluster in the FCM algorithm. The membership function is evaluated by minimizing an objective function [25]

$$J(U,V) = \sum_{\zeta=1}^{N}\sum_{c=1}^{C}\mu_c(\zeta)^{\alpha}\|X_\zeta - V_c\|^2,\ 1 \le \alpha \le \infty. \tag{18}$$

When the FCM converges, the *N* datasets are grouped into *C* clusters.

In this paper, the numbers of clusters (*C*) for the PPV or PD are 4 and 10, respectively. The center V_c of cluster *c* corresponds to the representative vector of this cluster and will be regarded as a state in the Markov model. The dimensions of both X_ζ and V_c are 1×1 and $N = 8760$.

B. Markov Model

The Markov model describes the probability, duration, and frequency of a state in a stochastic process [26], [27]. For a random Markov process, the probability, which irradiance/load at a generic instant falls into a state, is a function of

TABLE I
WEATHER STATISTICS IN LOCATION (23°47′, 120°96′)

	Spring	Summer	Autumn	Winter
	W/m²	W/m²	W/m²	W/m²
mean	1121.33	1130.85	1116.98	1094.72
σ	789.87	782.34	772.63	754.19

TABLE II
MARKOV MODEL OF PV POWER GENERATION

State (s_1)	1	2	3	4
Power (MW)	0.0	0.27	0.56	1.00
Prob.	0.12	0.11	0.09	0.67
Rate of departure	0.83	0.71	0.77	0.17
Freq. (oc/h)	0.08	0.07	0.08	0.12
Duration (h)	1.2	1.4	1.3	5.9

TABLE III
MARKOV MODEL OF LOAD DEMAND

State (s_2)	1	2	3	4	5	6	7	8	9	10
Demand (MW)	1.415	1.619	1.816	1.997	2.201	2.400	2.587	2.796	3.014	3.274
Prob.	0.02	0.08	0.12	0.13	0.11	0.12	0.12	0.11	0.10	0.09
Rate of departure	0.21	0.33	0.44	0.54	0.63	0.56	0.46	0.44	0.43	0.24
Freq. (oc/h)	0.00	0.03	0.05	0.07	0.07	0.07	0.06	0.05	0.04	0.02
Duration (h)	4.80	3.01	2.29	1.85	1.60	1.78	2.19	2.26	2.33	4.25

irradiance/load taken in a number of previous instants, which define the order of a Markov chain [26], [27]. In a first-order Markov chain, the irradiance/load at the current hour depends solely on the irradiance/load in the previous hour. The first-order Markov chain is well adopted in existing methods [28], [29]. Shamshad *et al.* showed that first- and second-order Markov chains for the meteorological data did not make any significant difference on the results because weather conditions usually change slowly in consecutive hours [30]. The load has similar characteristics in a distribution system. The states of PV power and load ($P_{\rm PV}$ or P_D) are gained by the FCM in Section III-A.

Let Pb_m, $m = 1, 2, \ldots, M$ be the probabilities associated with *M* states of a component (such as P_{PV} or P_D). Then

$$\sum_{m=1}^{M} Pb_m = 1 \tag{19}$$

$$[Ts]\,[Pb_1 \ldots Pb_M]^t = 0. \tag{20}$$

The upper triangle part of the $M \times M$ matrix [*Ts*] is composed of the repair rates among states while the lower triangle part consists of the failure rates. Each diagonal term of [*Ts*] equals the negative sum of all off-diagonal terms in the same column. The absolute value of the diagonal term for state *m* in (20) is defined as the *rate of departure* of state *m*. Three essential parameters of a state for a component are attained as follows.

1) Probability: Solve (19) and (20).
2) Duration: Reciprocal of individual rate of departure.
3) Frequency: Individual probability divided by its corresponding duration.

Once the Markov states of $P_{\rm PV}$ and P_D have been separately obtained, scenarios can be aggregated using different Markov states to attain the probabilities, durations, and frequencies of all scenarios. Suppose that the $P_{\rm PV}$ and P_D have *C*1 and *C*2 states, respectively. Then, $C1 \times C2$ scenarios can be obtained. The probability, duration, and frequency of a scenario can be calculated as follows.

1) The product of the probabilities of any two states yields the probability of a scenario.
2) The rate of departure of a scenario is the sum of the rates of departure of any two states. The reciprocal of the rate of departure for this scenario is its duration.
3) The frequency of a scenario is estimated by its probability divided by its duration.

In this paper, the hourly irradiations (leading to PV powers) in a location (latitude 23°47′ N, longitude 120°96′ E) in Taiwan were studied. The mean values and standard deviations (σ) of irradiance in four seasons are shown in Table I. The value of *C*1 is initiated from a reasonable one and is increased to one that results in a probability closed to zero. The maximum number of clusters implies the most appropriate clustering in the viewpoint of accuracy. The maximum number of clusters for *C*1 is 4 (i.e., $s_1 = 1, 2, \ldots, 4$), indicating a probability of 0.7 related to the rated power generation of 1 MW, as shown in Table II. The data indicate that the irradiance in this area is very strong. If other values of *C*1 are assigned (e.g., 5, 6, and 7), several probabilities become nearly zeros. In general, if a season in an area has a large range of irradiances, then the number of clusters is large. The proposed method utilizes hourly mean values of irradiances; cloudy conditions have an impact on the standard deviation of irradiance, which is not considered herein.

The IEEE reliability test data (8760 h loads) were utilized [31]. Again, a large number of clusters will result in a good accuracy. However, if the number of *C*2 is increased to be greater than 10, then one of the probabilities become very close to zero for these 8760 h loads. Consequently, the value of *C*2 is 10 ($s_2 = 1, 2, \ldots, 10$), as shown in Table III. Forty scenarios are thus investigated. Let $S = C1 \times C2$, $s = 1, 2, \ldots, S\,(= 40)$.

The failure rate and repair rate for the irradiance are 0.02–0.83 and 0.02–0.36, respectively. The failure rate and repair rate for the load are 0.01–0.22 and 0.01–0.26, respectively.

C. New Formulation Based on Markov Model

The cost of energy losses in (6) can be reformulated using the Markov models as follows:

$$\begin{aligned}\text{CEloss} = &\sum_{S \in \text{Sdis}} f(s) \times \text{Tdis} \times d(s) \times \text{Ploss}(s) \times C_{pk} \\ &+ \sum_{S \varepsilon \text{Sch}} f(s) \times \text{Tch} \times d(s) \times \text{Ploss}(s) \times C_{opk}.\end{aligned} \tag{21}$$

If the numbers of scenarios for discharging and charging are 24 and 16, respectively, then Tdis = 5694 and Tch = 3066. Specifically, *f*(s)×Tdis is the total number of times that the

TABLE IV
NUMBERS OF VARIABLES AND CONSTRAINTS IN CHRONOLOGICAL MODEL (8760 h) AND MARKOV MODELS (40 SCENARIOS)

	Variables or Constraints	Numbers
1	$P_B^{ch}(n,h)$	18396
	$P_B^{ch}(n,s)$	96
2	$P_B^{dis}(n,h)$	34164
	$P_B^{dis}(n,s)$	144
3	$E_B(n,h)$	52560
	$E_B(n,s)$	240
4	Sets of hourly power flow equations	8760
	Sets of power flow equations indexed by s	40
5	$E_B(n,h+1)=E_B(n,h)+\eta\times P_B^{ch}(n,h)- P_B^{dis}(n,h)$	52560
	$E_{DS}(n,s') = \sum_{s\epsilon Sdis+Sch} (E_{DS}(n,s) + d(s)P_{DS}^{ch}(i,s) - d(s)P_{DS}^{dis}(n,s)) \times t(s,s')$	240
6	$E_{DS}^{min}(n) \le E_{DS}(n,h) \le E_{DS}^{rated}(n)$	52560
	$E_{DS}^{min}(n) \le E_{DS}(n,s) \le E_{DS}^{rated}(n)$	240
7	$0 \le P_B^{dis}(n,h) \le P_B^r(n)$	34164
	$0 \le P_B^{dis}(n,s) \le P_B^r(n)$	144
8	$0 \le P_B^{ch}(n,h) \le P_B^r(n)$	18396
	$0 \le P_B^{ch}(n,s) \le P_B^r(n)$	96

discharging scenario s occur. $f(s)\times$Tdis$\times d(s)$ is the total duration of discharging scenarios.

The NPV of the arbitrage benefit in (7) becomes

$$\sum_{n=1}^{NB}\left(\sum_{s\in \mathrm{Sdis}} p(s)\cdot d(s)\cdot P_B^{\mathrm{dis}}(n,s)\cdot C_{pk} - \sum_{s\in \mathrm{Sch}} p(s)\cdot d(s)\cdot \frac{P_B^{\mathrm{ch}}(n,s)}{\eta}\cdot C_{opk}\right)\cdot \mathrm{PVF}. \quad (22)$$

Specifically, $\sum_{s\in \mathrm{Sdis}} p(s)\times d(s)\times P_B^{\mathrm{dis}}(n,s)$ is the expected value of discharged energy by the nth BESS in scenario s.

In the chronological study, the hour is repeatedly increased by one but the scenario stochastically shifts to any other in the union of Sdis and Sch. Let the transition rate (λ or μ) between scenario s and s' be $t(s, s')$. Then, (10) can be reformulated as follows:

$$E_B(n,s') = \sum_{s\in \mathrm{Sdis}\cup \mathrm{Sch}} (E_B(n,s) + d(s)\cdot \eta\cdot P_B^{\mathrm{ch}}(n,s) - d(s)\cdot P_B^{\mathrm{dis}}(n,s)\cdot t(s,s'). \quad (23)$$

D. Numbers of Variables and Constraints

In this paper, six BESSs in a distribution system are studied. Accordingly, NB = 6, $n = 1, 2, \ldots,$ NB. As described in Section II-A, if the system load exceeds a certain level (threshold), then the BESS discharges energy; otherwise, it charges. Assume that all BESSs are charging in 16 scenarios and discharging in 24 scenarios. Table IV shows the numbers of variables and constraints in the chronological model ($h = 1, 2, 3, \ldots,$ 8760) and the Markov model ($s = 1, 2, 3, \ldots, 40$). The numbers of both hourly variables and constraints are substantially reduced by using the Markov models.

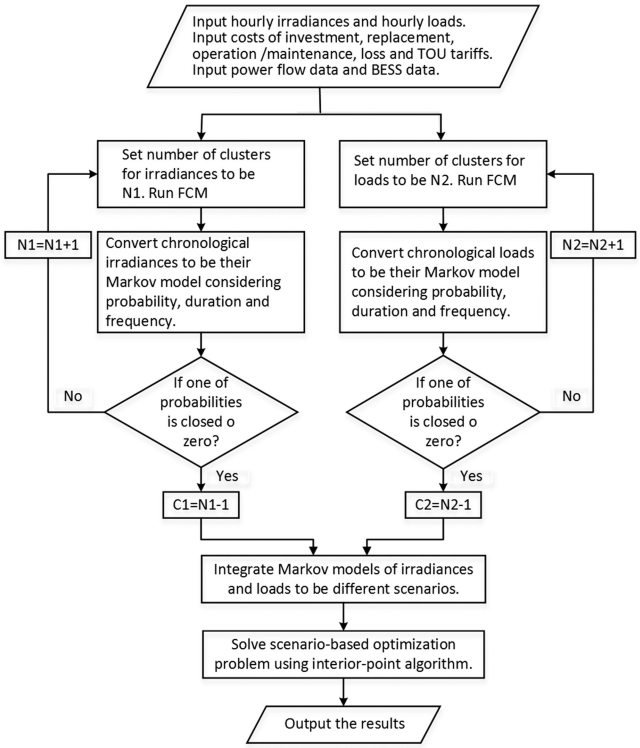

Fig. 3. Schematic flowchart of the proposed method.

To solve the above problem, a nonlinear programming method based on the interior-point algorithm [32] was used herein. The interior-point approach applied to constrained minimization solves a sequence of approximate minimization problems [33].

Fig. 3 shows the schematic flowchart of the proposed method. The numbers of clusters for irradiances and loads are set initially to $N1$ and $N2$, respectively. When one of probabilities becomes closed to zero, the appropriate $C1$ or $C2$ is obtained. Once both $C1$ and $C2$ are gained, the studied scenarios can be aggregated using different Markov states to attain the probabilities, durations, and frequencies of all scenarios. Finally, the interior-point approach applied to solve the scenario-based optimization problem.

IV. SIMULATION RESULTS

A 33-bus distribution system was used as a test system to show the applicability of the proposed method, as shown in Fig. 4 [34]. One PV farm of 1 MW is located at bus 18 and candidate buses for allocating BESSs include buses 16, 17, 21, 22, 25, and 32 [20].

A. Forty Scenarios

According to Tables II and III in Section III-B, 40 scenarios that occur in a year can be attained as shown in Table V by integrating individual information from PV and demand. A demand threshold can be set to define charging and discharging scenarios. For example, if the system demand exceeds 2 MW, then the BESS is in the discharging mode; otherwise, it is in

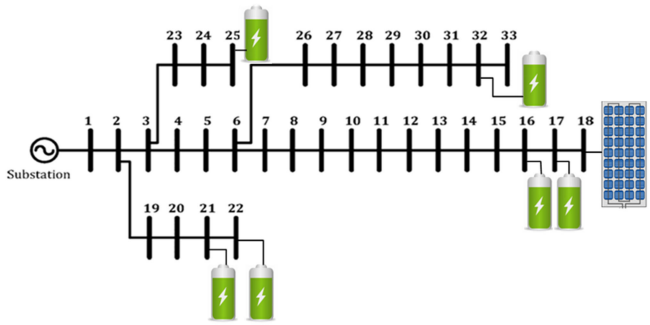

Fig. 4. 33-bus distribution system.

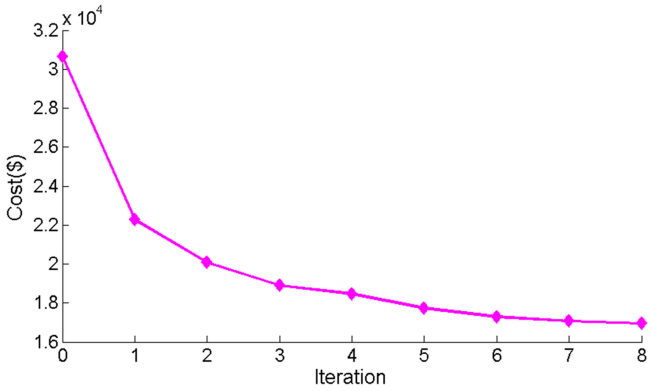

Fig. 5. Convergence of algorithm.

TABLE V
DATA FOR FORTY SCENARIOS

s	PV (MW)	Demand (MW)	Prob.	Freq. (Occ./h)	Duration (h)
1	0	1.415	0.002	0.002	0.990
2	0	1.619	0.008	0.009	0.885
3	0	1.816	0.012	0.015	0.806
4	0	1.997	0.013	0.017	0.746
5	0.27	1.415	0.002	0.002	1.099
6	0.27	1.619	0.008	0.008	0.971
7	0.27	1.816	0.012	0.014	0.877
8	0.27	1.997	0.013	0.016	0.806
9	0.56	1.415	0.002	0.002	0.990
10	0.56	1.619	0.008	0.009	0.885
11	0.56	1.816	0.012	0.015	0.806
12	0.56	1.997	0.013	0.017	0.746
13	1.00	1.415	0.014	0.006	2.439
14	1.00	1.619	0.056	0.030	1.887
15	1.00	1.816	0.084	0.054	1.563
16	1.00	1.997	0.091	0.067	1.315
17	0	2.200	0.011	0.016	0.699
18	0.27	2.200	0.011	0.015	0.752
19	0.56	2.200	0.011	0.016	0.699
20	1.00	2.200	0.077	0.064	1.205
21	0	2.400	0.012	0.016	0.735
22	0	2.587	0.012	0.015	0.794
23	0	2.796	0.011	0.014	0.806
24	0	3.014	0.010	0.012	0.813
25	0	3.274	0.009	0.009	0.962
26	0.27	2.400	0.012	0.015	0.794
27	0.27	2.587	0.012	0.014	0.862
28	0.27	2.796	0.011	0.013	0.877
29	0.27	3.014	0.010	0.011	0.885
30	0.27	3.274	0.009	0.008	1.064
31	0.56	2.400	0.012	0.016	0.735
32	0.56	2.587	0.012	0.015	0.794
33	0.56	2.796	0.011	0.014	0.806
34	0.56	3.014	0.010	0.012	0.813
35	0.56	3.274	0.009	0.009	0.962
36	1.00	2.400	0.084	0.064	1.316
37	1.00	2.587	0.084	0.055	1.515
38	1.00	2.796	0.077	0.049	1.563
39	1.00	3.014	0.070	0.044	1.587
40	1.00	3.274	0.063	0.028	2.273

the charging mode. Accordingly, the first 16 scenarios ($s = 1, 2, \ldots, 16 \in$Sch) involve charging and the other 24 scenarios ($s = 17, 18, \ldots, 40 \in$Sdis) involve discharging.

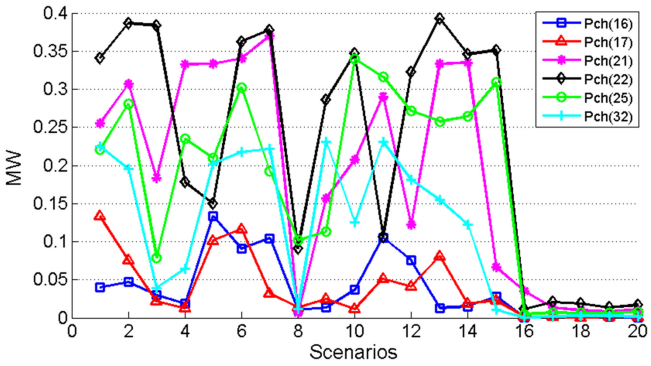

Fig. 6. MW charging of 6 BESSs in 20 scenarios.

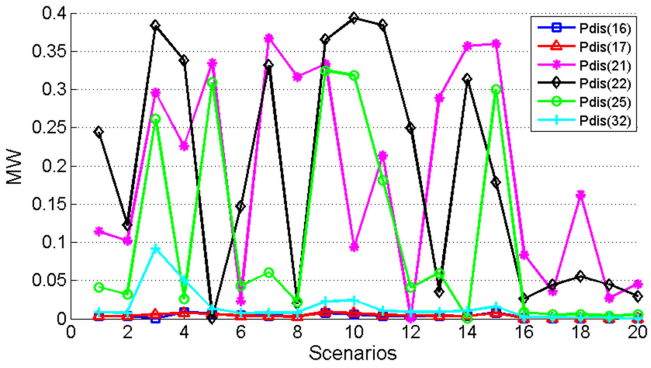

Fig. 7. MW discharging of 6 BESSs in 20 scenarios.

B. 20 Charging Scenarios and 20 Discharging Scenarios

To demonstrate the performance of the proposed method, the system demand threshold is set to 2.2 MW: if the system demand is smaller than 2.2 MW, then the TOU tariff is 18 \$/MWh and the BESS is charging; otherwise, TOU = 27 \$/MWh and the BESS is discharging. Thus, scenarios s, $s = 1$–20 ($\in$Sch), involve charging while the other 20 scenarios ($\in$Sdis) involve discharging. The efficiencies of the charging and discharging of BESS are 0.85 and 1.0, respectively.

As shown in Fig. 5, the interior-point algorithm takes eight iterations to converge. Figs. 6–8 display $P_B^{\mathrm{ch}}(n,s)$, $P_B^{\mathrm{dis}}(n,s)$, and $E_B(n,s)$, respectively. As depicted in Fig. 8, all BESSs in the first 20 scenarios are in their charging modes, yielding MWh

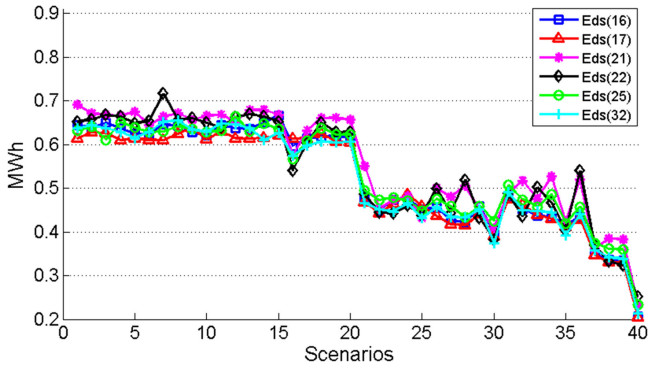

Fig. 8. Energies (MWh) of 6 BESSs in 40 scenarios.

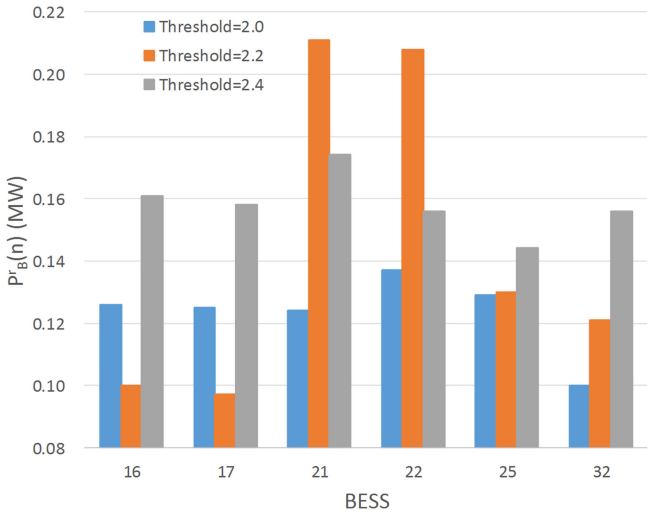

Fig. 9. Capacity rating $P_B^r(n)$ at different buses.

values within [0.53, 0.72]; the MWh values in scenarios s, $s = 21, 22, \ldots, 40$, are in the range of [0, 0.55].

C. Comparison of Different Numbers of Charging/Discharging Scenarios Under TOU

The demand threshold affects the TOU setting and the charging/discharging modes of BESS. This section investigates the different demand thresholds: 2.0, 2.2, and 2.4 MW, which result in 16, 20, and 24 charging scenarios (and 24, 20, and 16 discharging scenarios). The efficiencies of the charging and discharging of the BESS are 0.85 and 1.0, respectively. If the system load is below the threshold, then the TOU tariff is 18 \$/MWh; otherwise it is 27 \$/MWh.

Figs. 9 and 10 present the capacity rating $P_B^r(n)$ and size rating $E_B^r(n)$, respectively. Table VI shows the NPV of the CEloss ($\mathrm{NPV_{LO}}$), the NPV of the arbitrage benefit ($\mathrm{NPV_{AR}}$) and the cost of all BESSs. As shown in Table VI, if the threshold increases, then the $\mathrm{NPV_{LO}}$ and cost of BESS decrease, while the $\mathrm{NPV_{AR}}$ increases; however, $\mathrm{NPV_{AR}}$ is much smaller than $\mathrm{NPV_{LO}}$ and the cost of the BESS.

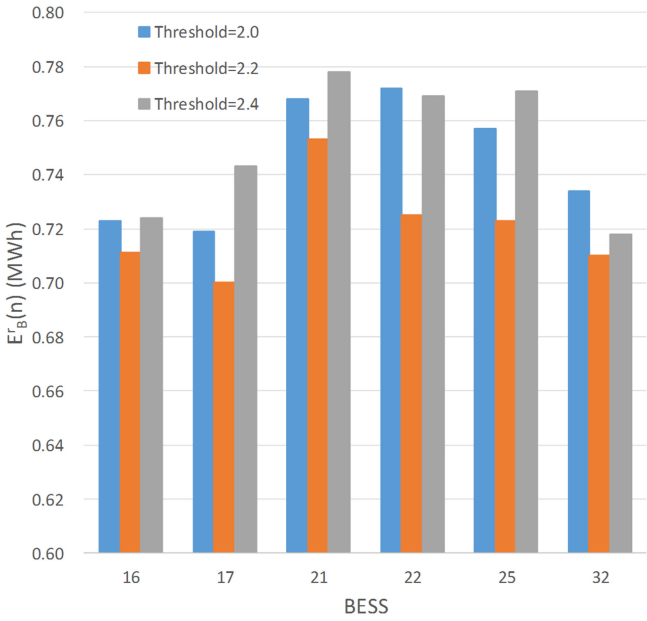

Fig. 10. Size rating $E_B^r(n)$ at different buses.

TABLE VI
COST COMPARISONS AMONG DIFFERENT CHARGING/DISCHARGING SCENARIOS

Load Threshold	2.0 MW	2.2 MW	2.4 MW
No. of Sch elements	16	20	24
No. of Sdis elements	24	20	16
NPV_{LO} (\$)	1.9945×10^4	1.6847×10^4	1.5904×10^4
NPV_{AR} (\$)	16.5290	20.8769	22.9423
Cost of BESS (\$)	2.0043×10^4	1.6934×10^4	1.5990×10^4

TABLE VII
COST COMPARISONS UNDER DIFFERENT TOU TARIFFS (DIFFERENT NUMBERS OF SCH/SDIS)

TOUs	18 \$/MWh and 27 \$/MWh	18 \$/MWh only	27 \$/MWh only
η	0.85	0.85	0.85
No. of Sch elements	16	16	16
No. of Sdis elements	24	24	24
NPV_{LO} (\$)	1.9945×10^4	1.3911×10^4	2.0524×10^4
NPV_{AR} (\$)	16.5290	25.9451	30.9503
Cost of BESS (\$)	2.0043×10^4	1.3992×10^4	2.0602×10^4

D. Comparison Among Different Numbers of Charging/Discharging Scenarios Under Uniform Tariff

This section explores the impact of TOU tariffs on the $\mathrm{NPV_{LO}}$, $\mathrm{NPV_{AR}}$ and cost of all BESSs. Two more uniform tariffs (18 \$/MWh only and 27 \$/MWh only) are studied. The numbers of Sch and Sdis are fixed at 16 and 24, respectively. As shown in Table VII, if only the low TOU tariff is considered, then the $\mathrm{NPV_{LO}}$ is small, so the cost of the BESS is low. In contrast, a high TOU tariff results in a high $\mathrm{NPV_{LO}}$ and a high cost of the BESS.

TABLE VIII
COST COMPARISONS UNDER DIFFERENT TOU TARIFFS
(SAME NUMBER OF SCH/SDIS)

TOUs	18 $/MWh and 27 $/MWh	18 $/MWh only	27 $/MWh only
η	1	1	1
No. of Sch elements	20	20	20
No. of Sdis elements	20	20	20
NPV_{LO} ($)	1.6847×10^4	1.2619×10^4	1.8965×10^4
NPV_{AR} ($)	20.8769	8.8405	13.3242
Cost of BESS ($)	1.6936×10^4	1.2718×10^4	1.9068×10^4

TABLE IX
COST COMPARISONS UNDER DIFFERENT TOU TARIFFS

TOUs	18 $/MWh and 27 $/MWh	18 $/MWh and 27 $/MWh
η	1	0.85
No. of Sch elements	20	20
No. of Sdis elements	20	20
NPV_{LO} ($)	1.6847×10^4	1.7373×10^4
NPV_{AR} ($)	20.8769	61.9176
Cost of BESS ($)	1.6936×10^4	1.7428×10^4

E. Comparison Among Same Numbers of Charging/Discharging Scenarios Under Various TOUs

This section explores the impact of TOU tariffs on the $\mathrm{NPV_{LO}}$, $\mathrm{NPV_{AR}}$ and cost of all BESSs. Two more uniform tariffs (18 $/MWh only and 27 $/MWh only) are studied. Both numbers of Sch and Sdis are fixed at 20 and both efficiencies of BESS charging/discharging are set to 1. As shown in Table VIII, if only the low TOU tariff is considered, then the $\mathrm{NPV_{LO}}$ is small and the cost of the BESS is also low. Besides, a high TOU tariff results in a high $\mathrm{NPV_{LO}}$ and a high cost of the BESS. That is, the TOU tariff dominates the results if the numbers of Sch and Sdis are the same.

F. Comparison Among Same Numbers of Charging/Discharging Scenarios Under Various Efficiencies of BESS Charging

In order to examine the impact of charging/discharging efficiencies of BESS on the $\mathrm{NPV_{LO}}$, $\mathrm{NPV_{AR}}$ and cost of all BESSs, this section sets $\eta = 1$ and 0.85. The TOU tariff are set to two prices; that is, 18 $/MWh for BESS charging and 27 $/MWh for BESS discharging. Both numbers of Sch and Sdis are fixed at 20. As shown in Table IX, a low charging efficiency results in a high $\mathrm{NPV_{LO}}$ and a high cost of the BESS if numbers of Sch and Sdis elements are the same.

V. CONCLUSION

This paper proposes a novel method for determining the optimal capacity (MW) and size (MWh) of battery energy storage systems at different buses in a distribution system. The novel contributions of this paper are summarized as follows.

1) The chronological hourly PV powers and loads over a year are transformed to be corresponding Markov models. The studied scenarios are obtained by integrating various Markov states of PV powers and loads.
2) The large number of chronological variables/constraints are reduced to a small number of scenario-based variables/constraints, to which an optimization method can be applied.
3) Instead of studying all scenarios individually, all scenarios can be optimized simultaneously in a single run by considering the probabilities, durations, and frequencies of all scenarios.

Some findings are given from the simulations.

1) The TOU tariff markedly affects the charging/discharging modes of BESSs and therefore the allocation of BESSs at various buses.
2) The annual arbitrage benefit is generally smaller than the costs of the BESSs and energy losses. A low (high) uniform TOU results in a low (high) cost of BESSs.
3) If the number of charging scenarios increases, then the $\mathrm{NPV_{LO}}$ and cost of BESS decrease, while the $\mathrm{NPV_{AR}}$ increases; however, $\mathrm{NPV_{AR}}$ is much smaller than $\mathrm{NPV_{LO}}$ and the cost of the BESS.

The future work consists of determination of candidate buses for installing the BESS and exploration of BESS as an ancillary service (spinning reserves or frequency regulation).

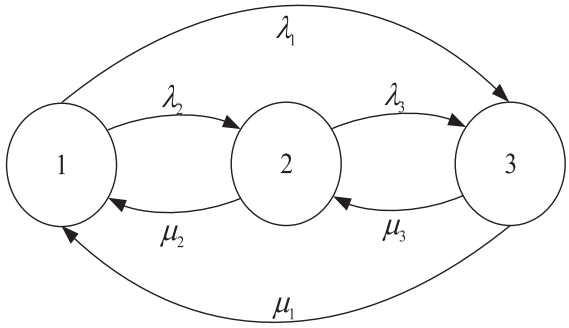

Fig. 11. Three-state markov model.

APPENDIX

This Appendix gives an example to obtain the failure rate (λ), the repair rate (μ) and probabilities of a three-state Markov model, as shown Fig. 11. The state transition matrix can be defined as follows:

$$[Ts] = \begin{bmatrix} -(\lambda_1+\lambda_2) & \mu_2 & \mu_1 \\ \lambda_2 & -(\mu_2+\lambda_3) & \mu_3 \\ \lambda_1 & \lambda_3 & -(\mu_1+\mu_3) \end{bmatrix}. \tag{A.1}$$

In order to attain the failure rate and the repair rate, the times form a state transited to any other state have to be counted in a given time-series, which consists of three states. Suppose that the times due to the state transition are given, as shown in Table X.

TABLE X
TIMES COUNTED BY TRANSITIONS AMONG STATES

From state / To state	State 1	State 2	State 3
State 1	1	2	3
State 2	3	1	4
State 3	2	4	3
Total	6	7	10

According to Table X, the probability transition matrix can be calculated as follows:

$$[Tp] = \begin{bmatrix} 1/6 & 2/7 & 3/10 \\ 3/6 & 1/7 & 4/10 \\ 2/6 & 4/7 & 3/10 \end{bmatrix}. \tag{A.2}$$

Thus, the state transition matrix is as follows:

$$[Ts] = \begin{bmatrix} -5/6 & 2/7 & 3/10 \\ 3/6 & -6/7 & 4/10 \\ 2/6 & 4/7 & -7/10 \end{bmatrix}. \tag{A.3}$$

According to (A.1), $\lambda_1 = 2/6,\ \mu_1 = 3/10,\ \lambda_2 = 3/6,\ \mu_2 = 2/7,\ \lambda_3 = 4/7,\ \mu_3 = 4/10$. According to (19) and (20)

$$[Ts]\,[Pb_1\ \ Pb_2\ Pb_3]^t = 0. \tag{A.4}$$

Thus, $Pb_1 = 0.2603$, $Pb_2 = 0.3390$, $Pb_3 = 0.4007$.

According to the above steps, it can be found that it is easy to solve a system of linear equations to find all probabilities, the failure rate, and the repair rate. However, any optimization method needs a long computer time to solve a problem. Reduction of the numbers of variables and constraints is crucial to improve the performance of optimization.

REFERENCES

[1] K. G. Boroojeni, M. H. Amini, and S. S. Iyengar, *Smart Grids: Security and Privacy Issues*. Cham, Switzerland, Springer, 2017.

[2] S. S. Iyengar and K.G. Boroojeni, *Oblivious Network Routing Algorithms and Applications*. Cambridge, MA, USA: MIT Press, 2015.

[3] K. G. Boroojeni, S. Mokhtari, M. H. Amini, and S. S. Iyengar, "Optimal two-tier forecasting power generation model in smart grids," *Int. J. Inf. Process.*, vol. 8, no. 4, pp. 79–88, 2014.

[4] S. Kar, G. Hug, J. Mohammadi, and J. M. F. Moura, "Distributed state estimation and energy management in smart grids: A consensus + innovations approach," *IEEE J. Sel. Topics Signal Process.*, vol. 8, no. 6, pp. 1022–1038, Dec. 2014.

[5] B. Currie *et al.*, "Flexibility is key in new york," *Power Energy Mag.*, May/Jun. 2017, vol. 15, no. 3, pp. 20–29, May/Jun. 2017.

[6] S. Repo *et al.*, "The IDE4L project," *Power Energy Mag.*, vol. 15, no. 3, pp. 41–51, May/Jun. 2017.

[7] J. Miller, *Understanding the Smart Grid: Features, Benefits and Costs*, Nat. Energy Technol. Lab., Dept. Energy, Washington, DC, USA, Jul. 8, 2008.

[8] M. Z. Daud, A. Mohamed, and M. A. Hannan, "An improved control method of battery energy storage system for hourly dispatch of photovoltaic power sources," *Energy Convers. Manage.*, vol. 73, pp. 256–270, 2013.

[9] M. Khalid and A. V. Savkin, Minimization and control of battery energy storage for wind power smoothing: Aggregated, distributed and semi-distributed storage," *Renewable Energy*, vol. 64, pp. 105–112, 2014.

[10] J. Quesada, R. Sebastián, M. Castro, and J. A. Sainz, Control of inverters in a low-voltage microgrid with distributed battery energy storage. Part II: Secondary control," *Elect. Power Syst. Res.*, vol. 114, pp. 136–145, 2014.

[11] J.W. Li, R. Xiong, Q. Q. Yang, F. Liang, M. Zhang, and W. J. Yuan, "Design/test of a hybrid energy storage system for primary frequency control using a dynamic droop method in an isolated microgrid power system," *Appl. Energy*, vol. 201, pp. 257–269, Sep. 2017.

[12] M. R. Andrea, L. da S. Armando, L. J. Jorge, and J. Carlos de Oliveira Mello, "Static and dynamic aspects in bulk power system reliability evaluations," *IEEE Trans. Power Syst.*, vol. 15, no. 1, pp. 189–195, Feb. 2000.

[13] L. Sigrist, I. Egido, and L. Rouco, "A method for the design of UFLS schemes of small isolated power systems," *IEEE Trans. Power Syst.*, vol. 27, no. 2, pp. 951–958, May 2012.

[14] M. Daghi, M. Sedghi, A. Ahmadian, and M. Aliakbar-Golkar, "Factor analysis based optimal storage planning in active distribution network considering different battery technologies," *Appl. Energy*, vol. 183, pp. 456–469, 2016.

[15] K. Mahani, F. Farzan, and M. A. Jafari, "Network-aware approach for energy storage planning and control in the network with high penetration of renewable," *Appl. Energy*, vol. 195, pp. 974–990, 2017.

[16] Y. Li, B. Feng, G. Q. Li, J. J. Qi, D. B. Zhao, and Y. F. Mu, "Optimal distributed generation planning in active distribution networks considering integration of energy storage," *Appl. Energy*, vol. 210, pp. 1073–1081, 2018.

[17] G. Mohsen and F. Hamid, "Battery capacity determination with respect to optimized energy dispatch schedule in grid-connected photovoltaic (PV) systems," *Energy*, vol. 65, pp. 665–674, 2014.

[18] R. Hemmati, H. Saboori, and M. A. Jirdehi, "Stochastic planning and scheduling of energy storage systems for congestion management in electric power systems including renewable energy resources," *Energy*, vol. 133, pp. 380–387, 2017.

[19] I. Kim, "Optimal capacity of storage systems and photovoltaic systems able to control reactive power using the sensitivity analysis method," *Energy*, vol. 150, pp. 642–652, 2018.

[20] A. S. A. Awad, T. H. M. EL-Fouly, and M. M. A. Salama, "Optimal ESS allocation for load management application," *IEEE Trans. Power Syst.*, vol. 30, no. 1, pp. 327–336, Jan. 2015.

[21] Y. J. Tang and S. H. Low, "Optimal placement of energy storage in distribution networks," *IEEE Trans. Smart Grid*, vol. 8, no. 6, pp. 3094–3103, Nov. 2017.

[22] A. Giannitrapani, S. Paoletti, A. Vicino, and D. Zarrilli, "Optimal allocation of energy storage systems for voltage control in LV distribution networks," *IEEE Trans. Smart Grid*, vol. 8, no. 6, pp. 2859–2870, Nov. 2017.

[23] M. Khaljani, R. K. Saray, and K. Bahlouli, "Comprehensive analysis of energy, exergy and exergo-economic of cogeneration of heat and power in a combined gas turbine and organic Rankine cycle," *Energy Convers. Manage.*, vol. 97, pp. 154–165, 2015.

[24] S. L. Wen, H. Lan, Y. Y. Hong, D. C. Yu, L. J. Zhang, and P. Cheng, "Allocation of ESS by interval optimization method considering impact of ship swinging on hybrid PV/diesel ship power system," *Appl. Energy*, vol. 175, pp. 158–167, Aug. 2016.

[25] J. C. Bezdek, R. Ehrlich, and W. Full, "FCM: The fuzzy c-means clustering algorithm," *Comput. Geosci.*, vol. 10, nos. 2/3, pp. 191–203, 1984.

[26] Y. Y. Hong and J. J. Wu, "Determination of transformer capacities in an industrial factory with intermittent loads," *IEEE Trans. Power Del.*, vol. 19, no. 3, pp. 1253–1258, Jul. 2004.

[27] T. Manco and A. Testa, "A markovian approach to model power availability of a wind turbine," in *Proc. IEEE Power Tech Conf.*, Lausanne, Switzerland, Jul. 2007, pp. 1256–1261.

[28] A. Bouabdallah, J. C. Olivier, S. Bourguet, M. Machmoum, and E. Schaeffer, "Safe sizing methodology applied to a standalone photovoltaic system," *Renewable Energy*, vol. 80, pp. 266–274, 2015.

[29] G. Carta, C. Grossi, and R. Manni, "Computer processing of the data required for the probabilistic forecasting of the daily peak power demand by means of Markovian processes," *IFAC Proc.*, vol. 12, no. 5, pt. 1, pp. 269–276, Sep. 1979.

[30] A. Shamshad, M. A. Bawadi, W. M. A. Wan Hussin, T. A. Majid, and S. A. M. Sanusi, "First and second order Markov chain models for synthetic generation of wind speed time series," *Energy*, vol. 30, pp. 693–708, 2005.

[31] Probability Methods Subcommittee, "IEEE reliability test system," *IEEE Trans. Power Apparatus Syst.*, vol. PAS-98, no. 6, pp. 2047–2054, Nov./Dec. 1979.

[32] S. Mehrotra, "On the implementation of a primal-dual interior point method," *SIAM J. Opt.*, vol. 2, pp. 575–601, 1992.
[33] Optimization Toolbox User's Guide, MATLAB, R2017a, MathWorks Inc., Natick, MA, USA, 2017.
[34] B. Venkatesh, R. Ranjan, and H. B. Gooi, "Optimal reconfiguration of radial distribution systems to maximize loadability," *IEEE Trans. Power Syst.*, vol. 19, no. 1, pp. 260–266, Feb. 2004.

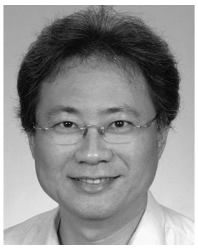

Ying-Yi Hong (SM'00) received the B.S.E.E degree from the Chung Yuan Christian University (CYCU), Taoyuan, Taiwan, in 1984, the M.S.E.E. degree from the National Cheng Kung University, Tainan, Taiwan, in 1986, and the Ph.D. degree from the National Tsing-Hua University, Hsinchu, Taiwan, in December 1990.

Sponsored by the Ministry of Education of R.O.C., he conducted research in the Department of Electrical Engineering, University of Washington, Seattle, from August 1989 to August 1990. He has been with CYCU since 1991. He was the Chair for the IEEE PES Taipei Chapter in 2001 and the Vice-Chair for the IEEE Taipei Section in 2013–2014. His research interests include power system analysis and AI applications.

Dr. Hong was the recipient of the Outstanding Professor of Electrical Engineering Award in 2006 from the Chinese Institute of Electrical Engineering (CIEE), Taiwan.

Man-Yin Wu received the B.S.E.E. degree from the Minghsin University of Science and Technology, Hsinchu, Taiwan, in 2014, and the M.S.E.E. degree from Chung Yuan Christian University, Taoyuan, Taiwan, in 2016.

Her research interests include the applications of evolutionary algorithms and smart grid.